Human Trabecular Meshwork Sphingolipid and Ceramide Profiles and Potential Latent Fungal Commensalism

Ayman J. Aljohani, Genea Edwards, Yenifer Guerra, Sander Dubovy, Darlene Miller, Richard K. Lee, and Sanjoy K. Bhattacharya

Bascom Palmer Eye Institute, University of Miami, Miami, Florida, United States

Correspondence: Sanjoy K. Bhattacharya, McKnight Vision Research Building, Bascom Palmer Eye Institute, University of Miami, 1638 NW 10th Avenue, Room 706A, Miami, FL 33136, USA; Sbhattacharya@med.miami.edu.

Submitted: November 7, 2013
Accepted: April 22, 2014

Citation: Aljohani AJ, Edwards G, Guerra Y, et al. Human trabecular meshwork sphingolipid and ceramide profiles and potential latent fungal commensalism. *Invest Ophthalmol Vis Sci*. 2014;55:3413–3422. DOI: 10.1167/iovs.13-13570

Purpose. We determined the profiles of sphingomyelin, sphingoid base, sphingoid base-1-phosphate, and ceramide, and their quantitative differences between control and glaucomatous trabecular meshwork (TM) derived from human donors.

Methods. Control and primary open angle glaucoma (POAG) TM samples were collected from cadaver donors. In addition, POAG TM surgical specimens also were procured. Lipid extraction was performed using suitable modifications of the Bligh and Dyer method. Protein concentrations were determined using Bradford's method. Lipids, identified using standardized class-specific lipid mass spectrometry, were quantified using a two-step ratiometric process. Gomori methenamine silver (GMS) staining was performed for detection of presence of *Fusarium* in the anterior eye tissue sections. PCR analyses were performed for detection of *Fusarium* species in the donor TM samples.

Results. Several species of sphingomyelin, sphingoid base, sphingoid base-1-phosphate, and ceramide were common between control and POAG TM. Only a subset of species in some of these classes were identified uniquely either in controls or in POAG TM. Several lipid species of fungal origin (many from Fungi imperfecti, *Fusarium* species) were found to be common between control and POAG TM. The GMS staining and PCR analyses showed presence of DNA belonging to *Fusarium* species suggesting latent commensalism.

Conclusions. Most sphingolipids and ceramides (except a few unique to a specific donor TM group) were found to be common in the control and POAG TM. Latent commensalism by *Fusarium* was suggested by identification of *Fusarium*-specific lipids, which was supported further by PCR amplification and sequencing of DNA.

Keywords: sphingolipid, ceramide, trabecular meshwork, lipidomics, glaucoma

Trabecular meshwork (TM) is a tiny filter-like region that exists at the iridocorneal angle in the anterior eye chamber and is involved actively in passage to aqueous humor (AH) in the normal eyes.[1] The TM shows an aberrant increased resistance in glaucoma resulting in impeded AH outflow and elevation in IOP, the key risk factor in glaucoma.[1] Glaucoma refers to a group of diseases characterized by progressive optic nerve degeneration. Primary open angle glaucoma (POAG) is the major prevalent type. It is the leading cause of irreversible blindness worldwide,[2] with an estimated 80 million affected people by 2020.[3]

Owing to its importance in glaucoma and POAG, the TM has been subjected to several structural,[4–7] proteomic (and/or compositional analyses),[8,9] and functional studies.[10] Although isolated studies of specific metabolites[11–13] and metabolism of selected lipids[14] have been carried out, a comprehensive metabolomic or lipidomic analyses of TM is largely lacking. Lipids often are major regulators of several cellular processes and also serve as bioactive signaling molecules[15–18] maintained under tightly regulated levels.[19] It is becoming evident that lipids have a significant role in homeostatic mechanisms in many biological systems.[20] Arguably, understanding composition and how the constituent molecules affect cellular behavior are keys to understanding the biology of TM, or for that matter any other tissue. The TM is characterized by elongated cells with relatively large interstitial spaces. Understanding the dynamic changes of TM is critical to understanding behavior of TM tissue and its aberration in the pathologic state.

Sphingolipids (and particularly sphingomyelin [SM] species) are found ubiquitously in the membranes of most cells, and have been shown to regulate many cellular and systemic events, including apoptosis, cell cycle, cellular growth, and inflammation.[18,19,21–24] Advancements in mass spectrometry and informatics approaches have removed two critical barriers toward high throughput identification and quantification[25] of lipids for performing lipidomics of the TM.[26,27] Until recently, the two critical barriers for high throughput lipidomics used to be the presence of several lipid species, each with very tiny amounts undetectable and unquantifiable by available methods and necessity of large amount of purified lipid for their unequivocal identification.[25,28–31] In this work, we sought to identify and quantify the sphingolipid and ceramide (Cer) profiles present in TM. We hypothesized that differences in age, race, individual health, and drug regimen will cause small variations in individual lipid species for a majority of sphingolipids, and we expected only a small subset of lipids to show relatively large changes between control and POAG TM samples. Since glaucoma is a multifactorial disease, incremental addition of many factors may influence the homeostatic balance of anterior eye segment tissues (and TM in particular) toward

pathologic conditions. Presence of incremental metabolic differences in a subset of TM sphingolipids may be possibly one such group of contributory factors. Are extraneous agents possible factors toward bringing incremental changes in TM sphingolipids in glaucoma? We present characterization of the molecular signature of four major sphingolipid species present in the human TM that includes cadaver-derived tissues as well as surgical TM specimens. Identification and relative quantification will pave the way for expansion of understanding of their role for the normal biology of TM cells and, by extension, that of the TM tissue.

Methods

Tissue Procurement

The POAG and control TM (Supplementary Table 1) were procured from cadaver donor eyes or as a surgical specimen (POAG) following institutional review board approved protocols and adherence to the tenets of the Declaration of Helsinki. The TM specimens, during transit, were stored in Optisol (Bausch & Lomb, Rochester, NY, USA) at 4°C followed by storage in −80°C until time of use. The donors of both sexes, and with a mean age of 55.9 ± 14.2 years for control and 70.2 ± 10 years for glaucoma, were used for these studies. Tissues were sourced from Midwest Eye-Banks, Lions Eye Bank (Miami, FL, USA) and Mundorf Eye Institute (Charlotte, NC, USA). The TM tissue was isolated using published procedures.[8]

Lipid Extraction

The TM tissue was subjected to an alternating cycle of freezing (−80°C) and thawing (37°C) for 10 minutes each for a total of five cycles (to break the membrane and release lipids) followed by extraction of lipids using the Bligh and Dyer method.[32] The organic phase, with extracted lipids, was dried in a Speed-Vac (Model 7810014; Labconco, Kansas City, MO, USA). Samples were flushed regularly with argon gas to prevent oxidation. The aqueous phase was subjected to protein quantification by the method of Bradford.[33] All extractions and subsequent handling were made using glass vials. A phosphatidylcholine standard (1,2-ditridecanoyl-sn-glycero-3-phosphocholine, molecular mass 649.9; Avanti Polar Lipids, Albaster, AL, USA) was added during tissue homogenization and its recovery was determined to calculate the extraction efficiency of each sample to normalize the recovery efficiency across the samples. These procedures are similar to those used for our published corneal and TM lipid extraction for phospholipids, and ensured uniform and > 99% recovery across all samples.[26,34]

Mass Spectrometric Analysis

The TSQ Quantum Access Max (Thermo Fisher Scientific, Pittsburgh, PA, USA) triple quadrupole electrospray mass spectrometer was used for analysis of lipids in infusion mode using TSQ Tune of Xcalibur 2.3 software suite. Extracted lipids were dried and resuspended in LC-MS grade acetonitrile/isopropanol (1:1). Samples were infused with a flow rate of 10 µL/min and analyzed for 2.00 minutes with a 0.500-second scan. The infusions were performed with Triversa Nanomate (Advion, Inc., Ithaca, NY, USA) controlled using Chipsoft 8.3.3 version with lipid class-specific optimal spray parameters. Briefly, SM and sphingoid base (SB) sprays were performed in positive ion mode with voltage of 1.55 kV and gas pressure of 0.45 psi; sphingoid base-1-phosphate (SB1P) and Cer in negative ion mode with voltage of 1.3 kV and gas pressure of 0.6 psi. Scans typically ranged from 200 to 1000 m/z unless specified otherwise. A fixed half peak width (FWHM) was set at 0.7 and collision gas pressure was set at 1 mTorr. Sheath gas (nitrogen) was set to 20 arbitrary units. Auxiliary gas (argon) was set to 5 arbitrary units. For analyses of sphingolipids and Cer collision energy, spray voltage and ion mode were set based on previous studies.[30,35] Briefly, the lipids of the SM, SB, and Cer classes were identified using neutral loss scan (NLS) for m/z 213.2, 48, and 256.2 with collision energies of 50, 18, and 32 V, respectively. Except for Cer, which was analyzed in negative ion mode, all others were scanned in positive mode. For SB1P, precursor ion scan (PIS) was performed in negative ion mode for product ion m/z of 79.1 using 24 V collision energy. We used class-specific lipid standards for quantification in a two-step process using procedures developed for automated lipid quantification.[30,36] Following standards were used: N-oleoyl-D-erythro-sphingosylphosphorylcholine, D-erythro-sphingosine, D-erythro-sphingosine-1-phosphate, and N-oleoyl-D-erythro-sphingosine (catalog numbers 860587, 860490, 860402, 860519; Avanti Polar Lipids) for ratiometric quantification of SM, SB, SB1P, and Cer, respectively. The molecular masses of these standards are 729.08, 299.5, 379.47, and 563.94, respectively. As first step, the abundant molecular species are quantified in a class-specific manner after isotopic correction in direct comparison of peak intensities with the added internal standard for each class. The abundant ions–based quantification then is used for quantification of less abundant ions in the second step.[25,30,36] Our current analyses used this two-step quantification approach, as this approach inherently takes into account that the ionization efficiencies of different lipid ions are different.[30] For each of the lipid classes, $n = 19$ control and $n = 20$ glaucomatous TM tissues were used (Supplementary Table 1). Approximately 5 scans each with and without internal standard (usually in the range of 0.1–2 pmol) were performed for each sample. The scans with internal standards were used for analyses. Those without internal standards were used for inspection and determination of reproducibility. To determine protein normalized lipid amounts, the aqueous phase–extracted proteins corresponding to organic phase lipids were subjected to protein quantification using the method of Bradford.[33] The total sphingolipids in the organic phase quantified by mass spectrometry were divided by total amount of protein (in µg), determined by the method of Bradford,[33] which was termed as protein normalized lipid amount. An aliquot of proteins in the aqueous phase (corresponding to organic phase with lipids) also was subjected to densitometric quantification using an amino acid quantified standard bovine serum albumin after fractionation and Coomassie blue staining on a PHAST gel[37] to ensure accuracy of quantification by the method of Bradford.[33] To confirm presence of a number of nonmammalian lipids, in particular, Fumonisins that were detected, we used additional parameters and procedures following published mass spectrometric studies (Supplementary Table 2).[38] The nonmammalian SB Fumonisins also were detected using a Q-Exactive (Thermo Fisher Scientific, Waltham, MA, USA) high resolution mass spectrometer connected to a Easy nLC nanospray LC system (using parameters for detection based on Orbitrap technology as described in a previously published report).[39] In general, we also have attempted to confirm all common nonmammalian lipids using a Q-Exactive-Easy nLC system that has been detected using TSQ Quantum Access Max instrument (Thermo Fisher Scientific) coupled to Nanomate described above.

Data Analysis, Ratiometric Quantification and Statistical Analysis

Representative spectra for each sample were inspected manually by two independent experienced observers from 5

Investigative Ophthalmology & Visual Science

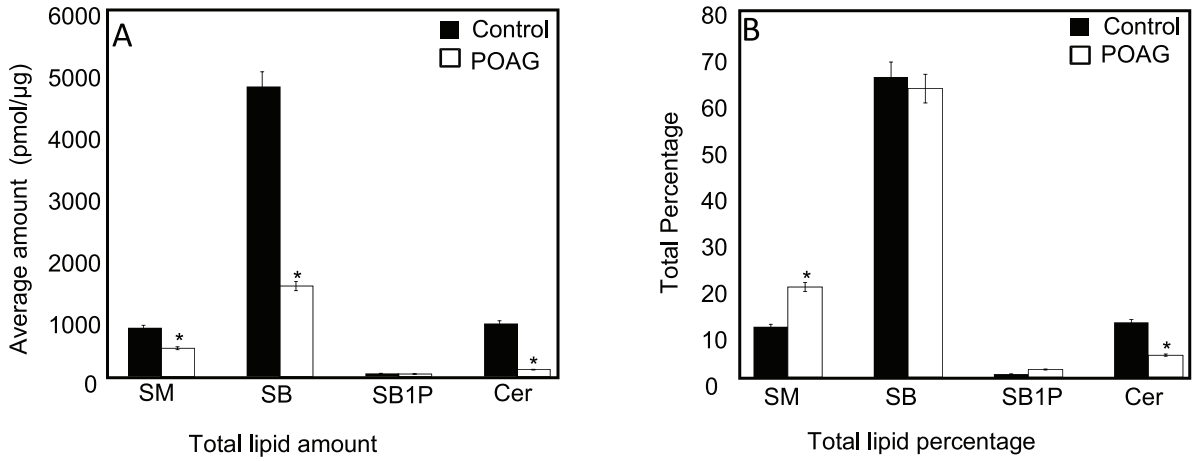

Figure 1. Composition of sphingolipids and Cers of control ($n = 20$) and POAG ($n = 20$) TM samples. (**A**) Amount of lipid species in pmol/µg of protein for sphingolipids (SM, SB, SB1P, and Cer) as indicated. (**B**) The same lipid species as in (**A**) expressed as percentage of total sphingolipids and Cers in each control and POAG TM. *Filled* and *hollow bars* represent control and POAG TM as indicated. A 2-tailed *t*-test was performed to compare quantities of lipids of each class between POAG and control groups. Statistically significant differences were found in lipid classes in POAG compared to control (*$P \leq 0.05$).

spectra, each collected with and without the internal standard for each sample. Spectra were imported into MZmine 2.9,[40] and analyzed after removal of noise (usually E2 levels). A file of the segment of database pertaining to specific lipid class to be analyzed was downloaded as *.csv file from LipidMaps (Lipidmaps structure database [LMSD], available in the public domain at www.lipidmaps.org) and used for lipid identification and quantitation using the MZmine 2.9 program. Protein amount (estimated from corresponding aqueous phase[25,26]) and normalized lipid amounts were determined, and comparison between control and POAG groups were performed using in-house written excel macros.[41] A 2-tailed *t*-test was performed to compare total quantities of lipids of each classes, measured by ratiometric quantification, between POAG and control groups. All unique lipid amounts (the amount of lipid pmol/mg protein) were found to be significantly different from 0.0 by the 1-sample *t*-test ($P \leq 0.05$). The selected common lipid species had statistically significant differences between the control and POAG groups by ANOVA. The Scheffe's post hoc test showed that they were statistically different ($P \leq 0.05$).

Gomori Methenamine Silver (GMS) Staining and PCR Detection for *Fusarium* Species

GMS staining was performed on paraffin-embedded tissue sections (8 µm) after deparaffinization of the tissue section following published protocols.[42]

For PCR analyses, the total genomic DNA was extracted from a portion of the tissues using the QIAGEN Kit (Invitrogen, Carlsbad, CA, USA). Primers F18S (5′-GCGGAGGGATCATTACC GAGTT-3′) and F28S (5′-CAGCGGGTATTCCTACCTGATC-3′) (Invitrogen) specific for *Fusarium* species targeting the internal transcribed spacer region, which included -ITS1, ITS2, and 5.8S; rRNA were selected and used to detect the presence of *Fusarium* species in ocular tissues. The PCR reactions were performed with approximately 50 ng of genomic DNA in a 25-µl PCR mixture, which included 1 µL (200 ng) of DNA template, 2.5 µL of buffer solution (containing the dNTPs and $MgCl_2$), 1 µL of each 10 µM primer (F18S and F28S), 1 µL of *Taq* DNA polymerase (Invitrogen), and 18.5 µL of distilled water. The PCR reactions were performed using the iCycler thermocycler (Bio-Rad, Hercules, CA, USA) with the following cycling parameters: 1 cycle at 95°C for 3 minutes, followed by 45 cycles with a denaturation step at 95°C for 30 seconds, an annealing step at 55°C for 30 seconds, and an extension step at 68°C for 2 minutes. A negative control was included in all experiments. The detection of amplified products (550 base pairs [bp]) was performed by electrophoresis of an aliquot of 5 µL of each amplicon in a 1% agarose gel with ethidium bromide 0.02% in 1 × Tris-acetate-EDTA (TAE) buffer. The DNA bands were visualized under UV illumination (Universal Hood II; Bio-Rad). A 1-kb molecular weight ladder (Invitrogen) was included in each run. The PCR products were purified with a spin kit (Geneclean; MP Biomedicals, Solon, OH, USA) according to the manufacturer's instructions. Amplified products were identified to the species level using direct sequencing and NCBI nucleotide blast. Direct sequencing of PCR products was performed by Genewiz, Inc. (South Plainfield, NJ, USA) with Big Dye version 3.1 (Applied Biosystems, Inc., Foster City, CA, USA). The reactions were run on a DNA analyzer (model 3730; Applied Biosystems, Inc.). The PCR amplification primers, F18S and F28S, were used as the sequencing primers, and the PCR products were sequenced on both strands in duplicate or triplicate to assure sequence fidelity.

Results

The ratiometric mass spectrometric quantification revealed a decrease in total amount of sphingolipids (SM, SB, SB1P) and Cers in glaucoma compared to control (Fig. 1A). The decrease was most pronounced in SB (but not in SB1P) and in Cers. To determine their relative level with respect to each other in the control and POAG groups, we also calculated their level in the group (control or POAG) as percentage of total aggregate of these four classes. Percentage of total lipids showed opposite trend for SM and SB1P, which are higher in POAG compared to controls (Fig. 1B). As percentage of total lipids, SB and Cers in the TM were found to be lower in POAG compared to control (Fig. 1B), similar to the trend found using total amounts (Fig. 1A). However, the difference was lower when the levels of SB and Cer were compared as percent of total lipids than as total amount.

We next looked into the side chain length distribution of each class of lipids, dividing them into five categories (acyl

Investigative Ophthalmology & Visual Science

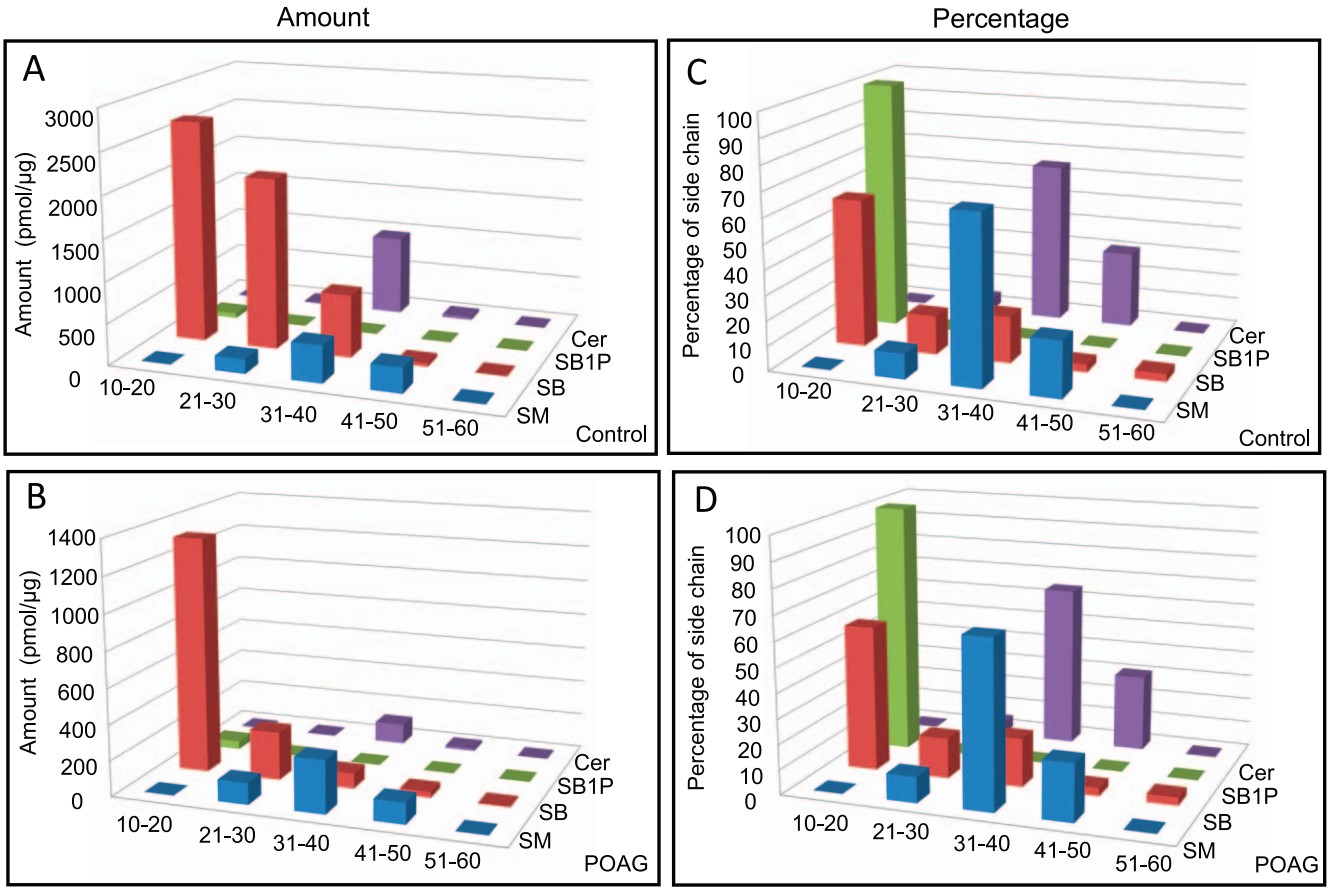

Figure 2. Composition of side chains of sphingolipids (SM, SB, SB1P, and Cer) in control ($n = 20$) and POAG ($n = 20$) TM samples. (**A**) Amount (pmol/µg of protein) of side chain containing sphingolipids and Cers in the control TM. (**B**) Amount (pmol/µg of protein) of specific side chain containing sphingolipids and Cers in the POAG TM as indicated. (**C**) The sphingolipids and Cers side chain in control samples expressed as percent of total lipids (total lipids in SM, SB, SB1P, and Cer classes). (**D**) The sphingolipids and Cers side chains in POAG samples expressed as percent of total lipids (total sphingolipid and Cers). Symbols are: SM SB SB1P Cer.

chain lengths of 10–20, 21–30, 31–40, 41–50, and 51–60; Fig. 2). Amount of lipids distributed by side chains of lipid species in each group (control of POAG) revealed a remarkable difference in the 10 to 20, 21 to 30, and 31 to 40 side chain species of SB, followed by 31 to 40 side chain containing Cers and SM species (Figs. 2A, 2B). In contrast, when expressed as the percent of total lipid, two groups (control and POAG) showed near identical distribution of side chain lipids in all four classes (Figs. 2C, 2D). However, compared to the total lipids either determined as amounts (normalized to protein) or percent of total lipids (Figs. 1A, 1B), the distribution of side chains in all four classes of lipids (Figs. 2C, 2D) is somewhat more revealing. The amount of side chain distribution is consistent (Figs. 2A, 2B) with lipids expressed as percent of total with respect to SM, where 31 to 40 acyl side chain length shows an increase in POAG and can account for an increased total percent of SM (Fig. 1B). Reverse trend of decreased Cer (Fig. 1B) also is consistent with side chain distribution in POAG (Figs. 2A, 2B). However, SB that shows very little change as percent of total (Fig. 1B) shows a significant decrease for side chain species 21 to 30 and 31 to 40, and even in the10 to 21 range, the amount is reduced by more than half in POAG (Figs. 2A, 2B). The increased SB1P observed as the percent of total lipids in POAG (Fig. 1B) is largely accounted for by an increase in 10 to 21 acyl side chain in SB1P species (Figs. 2A, 2B). We next made an attempt to look into individual lipids in each lipid class.

SM Species

Quantitative mass spectrometric analysis of SM species in the human TM revealed only three SM species uniquely present in control samples and only one species present uniquely in glaucoma samples (see Table). The control and POAG donors showing unique SM species (see Table) showed other confounding factors, such as disease, lipid related metabolic disorder, or history of smoking (Supplementary Table 1). In contrast, we found 46 SM species to be present in control and glaucoma (Fig. 3, Supplementary Table 3). Only a handful of species that are common between control and glaucoma undergoes any dramatic change, most notable being SM (d17:1/24:1) in the control group that undergoes a dramatic decrease followed by SM (d18:1/12:0; Fig. 3, Supplementary Table 3). In the POAG group, SM (d18:1/16:1) showed an increase compared to control (Fig. 3, Supplementary Table 3). The SM species common between control and POAG, however, are a tiny fraction of total sphingolipids and Cers (Fig. 1, Supplementary Fig. 1).

SB Species

Quantitative analysis of SBs uniquely identified a single nonmammalian species, Prosopinine, in the control TM sample (see Table); the donor had a history of diabetes (Supplementary Table 1). A total of 31 SB species was present in control as well as POAG TM samples (Fig. 3, Supplementary Table 4). A

Table. Unique Lipid Species in the TM

	Sphingomyelin Species							
Lipid Species*	**Number of Isomers**	**Exact m/z**	**m/z,† [M+H]+**	**Actual m/z**	**Error, Da**	**Average Lipid Amount‡**	**SEM**	**Donor Frequency**
Control								
SM(d16:1/20:1)	7	728.5	729.5	729.9	−0.4	5.44	1.08	2
SM(d18:0/18:0)	2	732.6	733.6	733.1	0.5	0.21	0.02	2
Glaucoma								
SM(d18:2/22:1)	N/A	782.6	783.6	783.4	0.2	5.68	0.42	3

* The lipid species identification is based on Lipidmaps database, used as a *.csv file for bioinformatic analyses with MZmine 2.9 program.

† A representative mass/charge ratio is presented (variations in m/z were reconciled by MZmine 2.9). Average standard non-normalized dataset is presented here. For some lipid species identified, standard deviation value could not be calculated due to lack of presence in all samples. Average lipid amount is pmol lipid per species/μg protein.

‡ All unique lipid amounts (the amount of lipid pmol/mg protein) were found to be significantly different from 0.0 by the 1-sample *t*-test ($P \leq 0.05$). The 7 isomers are: SM(d18:1/18:1(9Z)), SM(d18:2/18:0), SM(d19:1/17:1), PE-Cer(d14:2(4E,6E)/25:0), PE-Cer(d15:2(4E,6E)/24:0), PE-Cer(d16:2(4E,6E)/23:0), PE-Cer(d16:2(4E,6E)/23:0). The two isomers are: SM(d16:0/20:0), SM(d19:0/17:0). The donor codes are: SC023, SC024; SC001, SC005, and SC049, SC056, SC057, respectively (Supplementary Table 1).

number of nonmammalian species, particularly the SB species of fungi imperfecti, such as fumonisin B2, B4, C1, and C3 (Supplementary Table 4), all products *Fusarium* species, were found to be prevalent and common among both groups (Fig. 3, Supplementary Fig. 1, Supplementary Table 4). As evident from total lipid analyses (Fig. 1), SB constitutes the largest proportion of lipids in these four classes of sphingolipids and Cers is corroborated further by distribution of common SBs (Fig. 3, Supplementary Table 4, Supplementary Fig. 1). A number of SBs in control tissue undergo a significant decrease in POAG. In contrast, only a single bona fide mammalian SB species, 6-hydroxysphingosine, has shown dramatic increased

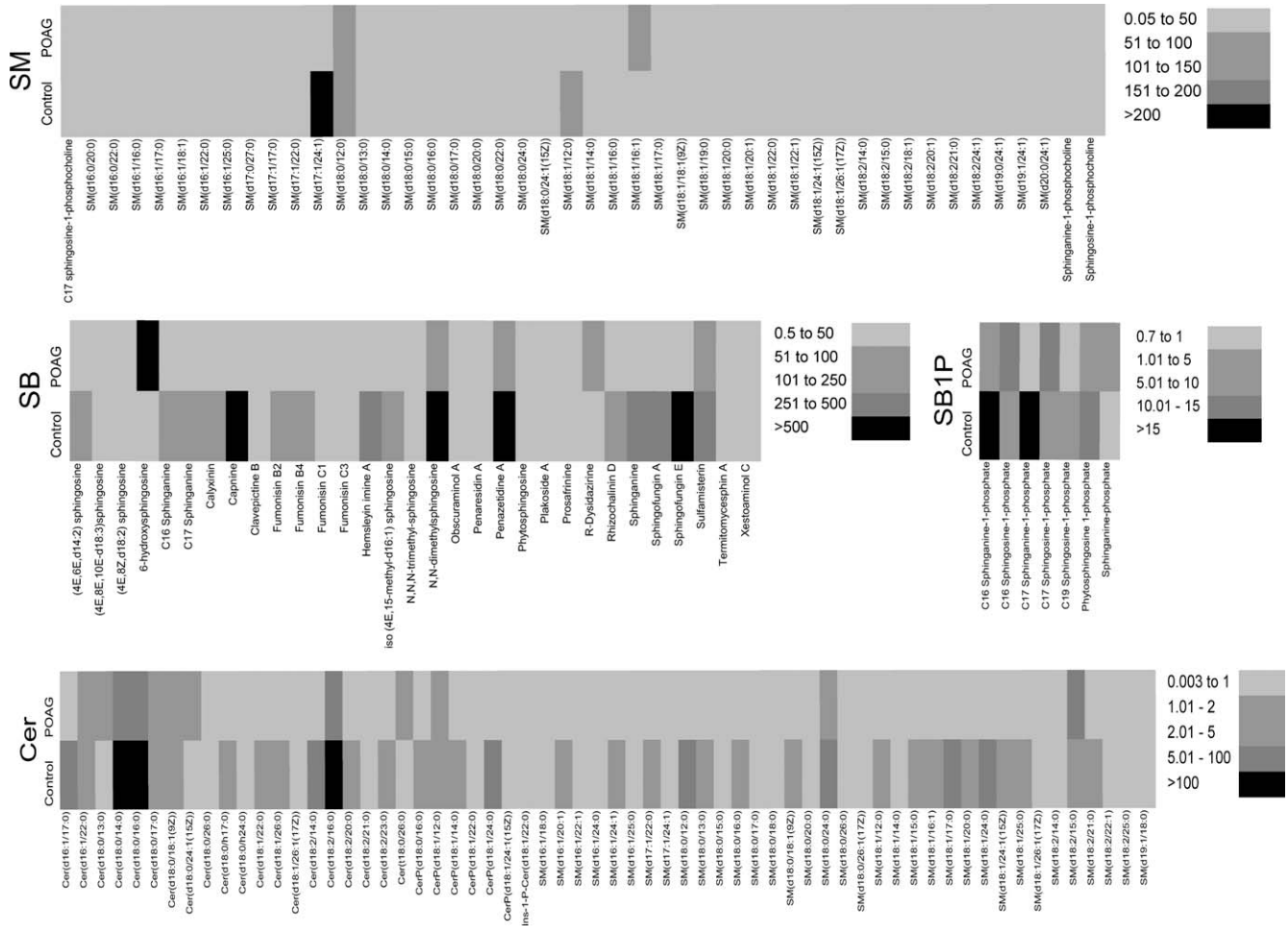

Figure 3. Heat map of sphingolipids (SM, SB, SB1P) and Cer species found common between control (total $n = 20$) and POAG (total $n = 20$) TM. Average amount of lipid (pmol/μg protein) have been presented. *Scale bar* of amounts used for given lipid species are as indicated.

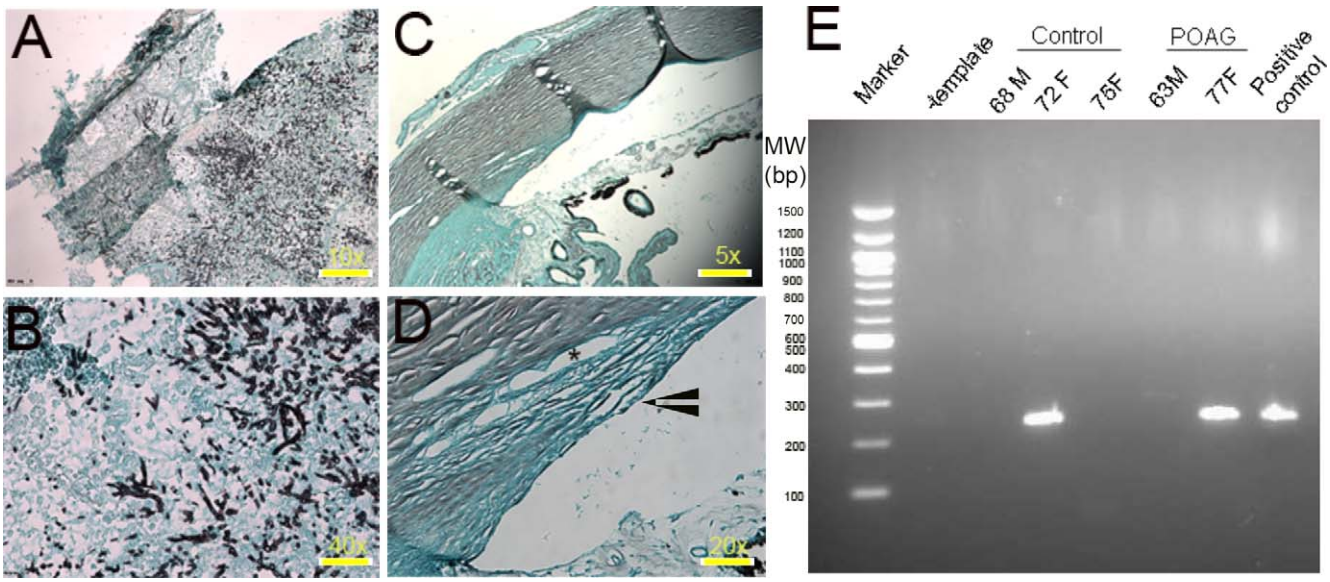

Figure 4. GMS staining and the PCR products to demonstrate presence of *Fusarium* species in human TM samples. (**A**, **B**) Represent a GMS-stained positive control for *Fusarium* species in different magnifications (×10 and ×40 as indicated), respectively. (**C**, **D**) Representative human POAG TM stained with GMS (magnification power ×5 and ×20 as indicated). *Arrowhead* and *star* represent TM and Schlemm canal, respectively. (**E**) The PCR amplified product of *Fusarium* species electrophoresed on agarose gel (2%) and stained with ethidium bromide. Control, POAG-derived products (all Caucasian donors, age, and sex, and a positive *Fusarium* sp. DNA as positive control) used are as indicated. A negative control lacked any DNA template (–template). Molecular weight marker sizes are as indicated. M, male; F, female.

levels in POAG compared to controls (Fig. 3, Supplementary Fig. 1, Supplementary Table 4).

SB1P Species

Only 7 SB1P species were identified in the human TM samples; all were common between control and glaucoma (Fig. 3, Supplementary Table 5, Supplementary Fig. 1). No SB1P species was found to be unique in either group. All except C16 SB1P, C17 SB1P, and sphinganine-phosphate (these three showed an increase) underwent a decrease in level in POAG (Fig. 3, Supplementary Table 5). The SB1P species represents the lowest percent for a class (Fig. 1, Supplementary Fig. 1) as a total percent of lipids among these four classes of lipids.

Cer Species

No Cer species was found unique between control and POAG; however, 62 Cers were common between these two groups (Fig. 3, Supplementary Table 6, Supplementary Fig. 1). The ceramides Cer(d18:0/14:0), Cer(d18:0/16:0), and Cer(d18:2/16:0) undergo a significant decrease in POAG compared to controls (Fig. 3, Supplementary Fig. 1, Supplementary Table 6), while approximately three species, Cer(d18:0/13:0), Cer(d18:0/24:1[15Z]), and SM(d18:2/15:0), show a marginal increase in POAG (Fig. 3, Supplementary Table 6).

Latent Commensalism of Fungi Imperfecti

Common occurrence of SB fumonisin B2, B4, C1, and C3 in control and POAG groups indicated possible local production of these lipids in the TM. Human TM tissue from control and POAG groups, subjected to GMS staining failed to reveal lack of fungi imperfecti or *Fusarium* fungi species (Figs. 4A–D). The PCR-amplified product using *Fusarium* species-specific primers amplified a DNA band comparable to size of the positive control (Fig. 4E). Subsequent sequencing (Supplementary Fig. 2) confirmed it to be bear *Fusarium* DNA sequence, supporting frequent presence of latent *Fusarium* species in the TM of either group.

Discussion

We present identification of sphingolipid and Cer species in the control and POAG TM. Identification and quantification of constituent molecules (nucleic acids, proteins, lipids, and metabolites) are important to understand structural organization and function of TM cells, as well as their aberration in pathologic states. A combination of surgical and cadaver POAG TM tissues were used for these analyses, similar to our previous proteomic analyses,[8] to rule out artifacts of postmortem changes.

We found decreased total amounts of sphingolipids (SM, SB, SB1P) and Cers in POAG compared to controls (Fig. 1A). The differences in total amounts of SM, SB, and Cers in POAG were found statistically significant than controls (Fig. 1A). Relative level in control and POAG as an aggregate of total percentage of these four classes showed an opposite trend for SM and SB1P, which were higher in POAG compared to controls (Fig. 1B). On the other hand, as percentage of total, SB and Cers in TM were found to be lower in POAG compared to controls (Fig. 1B), similar to the trend found for the total amounts of these species (Fig. 1A). The SM and Cers were found to be statistically significant when compared as an aggregate of total percentage (Fig. 1B).

The side chain distribution of lipid species (as total amount normalized to proteins) in control and POAG tissues revealed a dramatic difference in 10 to 20, 21 to 30, and 31 to 40 side chain species of SB, followed by 31 to 40 side chain containing Cers and SM species (Figs. 2A, 2B). In contrast, near identical distribution of side chain lipids in all four classes were observed when expressed as the percent of total lipid within control and POAG groups (Figs. 2C, 2D) suggesting that, while the total lipids undergo a decrease (Fig. 1A), the relative distribution of lipids containing different side chain lengths is

Investigative Ophthalmology & Visual Science

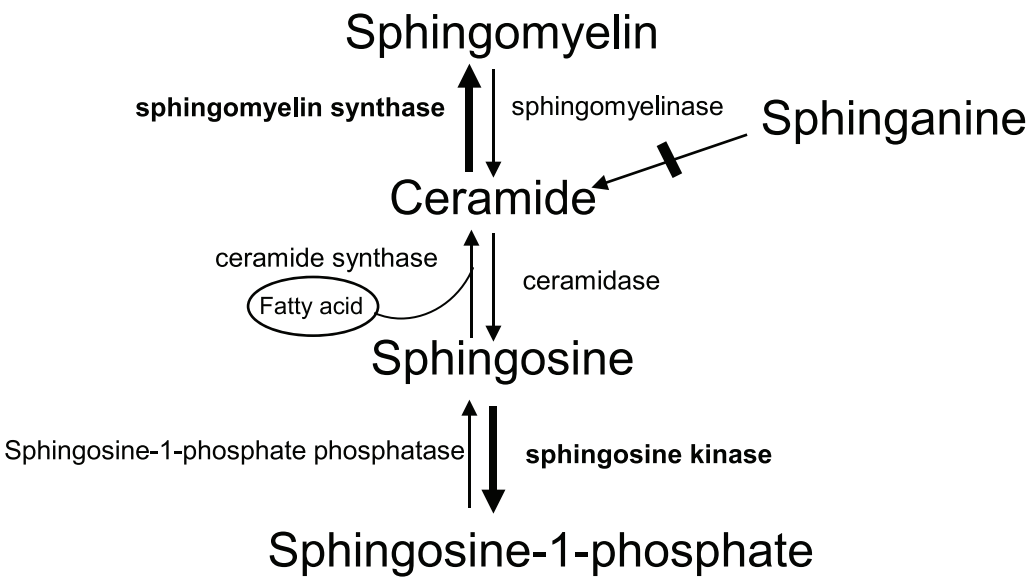

Figure 5. A schematic pathway diagram of conversions between sphingolipid and Cer species. *Bold arrow* suggests that this direction is a likely possibility in POAG. The *step* depicted by *dotted arrow* suggests that this process may be substantially decreased in POAG.

not an across-the-board uniform reduction of all lipid species within each class (Figs. 2A, 2B).

The SM, SB, its monophosphate derivatives, and Cers can be generated by interconversions (Fig. 5) and, consequently, multiple modalities and aberration in enzymatic activities may result in a high amount of one or more of these lipid species in the pathologic state compared to controls.

Glaucoma affects a large number of people worldwide, with wide variations in ethnicity and environment.[3] It is plausible that multiple factors in various combinations may precede the pathology, which may vary among glaucoma patients. Addition of small incremental changes of several factors (from a baseline in the normal state) may impact the homeostatic balance of TM tissue toward pathologic changes leading to glaucoma. The incremental differences in levels and species of TM sphingolipids may be a part of such contributory factors. Biochemical individuality of the donors has been found previously as a singular important contributor to presence of specific unique lipids in donor tissues for TM phospholipids,[26] cholesterol, and glycosphingolipids,[27] and the same possibility exists for sphingolipids. Systemic diseases or disorders, for example, hyperlipidemia; use of lipid modulating drugs, such as statins; and other confounding factors or nonsystemic diseases are possible factors, which may contribute to biochemical individuality.

The presence of only few unique SM species in control or POAG TM (see Table) is consistent with our hypothesis that only small differences with respect to unique species are expected between control and POAG. Importantly, the unique species either in control or POAG are present only in a limited number of donors. Lack of frequency is suggestive of biochemical individuality of the donors rather than their association with glaucoma (see Table). However, their association with a subset of POAG cannot be ruled out either. Myocilin mutations also are associated with a very limited subset of POAG, estimated to be in less than 5% of total worldwide POAG population.[43]

The mammalian SM species SM(d16:1/20:1), SM(d18:0/18:0), and SM(d18:1/18:0) were found uniquely in the control group, while SM(d18:2/22:1) was identified uniquely in POAG TM tissue (see Table). These species have been reported in detergent-resistant membranes,[44] and in aberrant cell surface glycocalyx,[45] but the specific function they serve remains unknown. We found approximately 12 SM whose level is significantly different between control and POAG groups (Supplementary Table 3), and their biological role in anterior eye chamber remains unknown.

The SB is the highest contributing class in terms of amount or relative percentage in total lipid encompassing sphingolipids and Cers (Fig. 1). We found all 31 SB species as common between control and POAG TM samples (Fig. 3, Supplementary Table 4). Interestingly a surprising number of nonmammalian SB species, particularly those belonging to fungi imperfecti, were detected. The SBs from *Fusarium* species, fumonisin B2, B4, C1, and C3 (Supplementary Table 4), were recurrently identified among the control and POAG groups (Fig. 3, Supplementary Fig. 1, Supplementary Table 4). Their levels were statistically significantly different between the POAG and control groups (Supplementary Table 4). To confirm presence of these fumonisin species in the TM, we used single reaction monitoring with a different collision energy to identify previously published diagnostic product ions[38] and precursor ions (Supplementary Table 2), or high resolution mass spectrometry using a Q-Exactive instrument and published parameters.[39]

Based on these findings, we questioned whether Ahmed, Baerveldt's glaucoma drainage implants, or a prolonged steroid treatment favored *Fusarium* infection or commensalism.[46,47] The GMS staining of the TM from several donors in either group did not show the presence of *Fusarium* or other fungi imperfecti (Figs. 4A–D). The PCR analyses revealed presence of *Fusarium* species the TM irrespective of control or POAG TM tissue. Sequencing of amplified products confirmed them belonging to *Fusarium* 18S rRNA (Supplementary Fig. 2). Taken together with presence of fumonisin variants, it is suggested that they are likely due to latent *Fusarium* infection in the TM tissue. Not all TM samples showed *Fusarium* species using PCR analyses, suggesting either a nonuniform infection or presence of *Fusarium* and, consequently, its DNA fragments below a threshold necessary for PCR detection. The presence of *Fusarium* rRNA amplicon is detected (Fig. 4E), but there is a lack of detection of *Fusarium* by staining (Figs. 4C, 4D), however, their potential local production of fumonisin species (Supplementary Table 4) suggests latent infection or commen-

salism rather than pathogenic presence. The production of fumonisin species, if, indeed, it occurred locally in the TM, would be indicative of a metabolically active organism rather than dormant organism. However, the detection of different fumonisin species in the TM derived entirely from food cannot be ruled out with our current analyses. A decade of investigation in agricultural chemistry has shown that fumonisin lipids are not entirely degraded by heating the food material and they can transfer to different mammalian tissue from food.[38,39,48] However, the presence of fumonisin lipids have been shown to alter the phospholipid profiles.[49] Our earlier analyses of changes in TM phospholipid profiles[26] will be consistent with alteration contributed by the presence of fumonisin lipids. Altered levels or species of sphingolipids and other lipids could be contributory biochemical factors that may alter the biochemical balance of TM tipping toward the development of ocular hypertension. Could extraneous factors, such as latent *Fusarium* generating very tiny amounts of fumonisin, contribute toward small incremental metabolic changes? The observations presented here suggest this possibility. Either a small secretion of fumonisin due to latent commensalism or due to their accumulation via absorption from the circulating fluids in the TM are possibilities, which has the potential to alter sphingolipid or phospholipid levels as evident from the published literature on other cells/tissues.[49]

The SBs (Figs. 1, 3; Supplementary Table 4; Supplementary Fig. 1) undergo a significant decrease in POAG. In contrast only a mammalian SB species, 6-hydroxysphingosine, and a non-mammalian R-dysidazirine show a dramatic increase in POAG compared to controls (Fig. 3, Supplementary Fig. 1, Supplementary Table 4).

The SB1P species, which are known chiefly for their role in cell signaling,[20,22] represented the lowest percent for a class (Fig. 1, Supplementary Fig. 1) as a total percent of lipids. No unique SB1P was uniquely detected in either control or POAG TM. All SB1P species recorded a decrease in level, four of them statistically significant in POAG compared to controls (Fig. 3, Supplementary Table 5). Exceptions were C16 sphingosine-1-phosphate, C17 sphingosine-1-phosphate, and sphinganine-phosphate, which showed an increased level in POAG. Not much is known about the functional role of these species. They have been ascribed to some neurodegenerative diseases, such as Alzheimer's,[50] only recently. Better integration of lipidomics with transcriptomics and proteomics, in future, is expected to provide insight into the role of these entities in cellular function.[51]

Cers are ascribed to have a role in apoptosis, death, and decay.[21,23,24] Despite the presence of 62 Cers in the TM (Fig. 3, Supplementary Table 6, Supplementary Fig. 1), no unique Cer was found in the POAG or control group. Significantly decreased level of Cer (d18:0/14:0), Cer(d18:0/16:0), and Cer(d18:2/16:0) was found in the POAG group compared to controls (Fig. 3, Supplementary Fig. 1, Supplementary Table 6). Conversely, three species, Cer(d18:0/13:0), Cer(d18:0/24:1[15Z]), and SM(d18:2/15:0), showed a marginal increase in POAG (Fig. 3, Supplementary Table 6). The role of these Cer species, either at the isolated TM cell or the TM tissue level, is not clear.

One limitation of studying lipid changes in human TM is obtaining TM tissue in hypertensive state. Thus, the comparison is between control and drug-induced post-IOP elevation when using human TM tissue. There is a lack of suitable model system that captures all features of human POAG simultaneously, offering a high degree of anatomic similarity with human TM. We recently have analyzed TM sphingolipids between normotensive and hypertensive states in a mouse (DBA/2J) model that develops spontaneous IOP elevation. This study has revealed unique sphingolipids in normotensive and hypertensive states.[52] The DBA/2J model shows heterogeneity with respect to onset and extent of IOP elevation, and often develops pigmentary dispersion in the anterior chamber. However, the IOP elevation in DBA/2J is inconsistent with amount of pigment dispersion (unpublished observations). The unique sphingolipids and Cers observed between normotensive and hypertensive mouse TM is different than in human TM presented here.[52] The number of unique sphingolipid species found between control and glaucomatous human TM (see Table) is much smaller than in mice,[52] which may be due to several factors, including system differences.

It is pertinent to note that the application of specific sphingolipids, such as sphingosine-1-phosphate has been known to decrease aqueous humor outflow.[53] To our knowledge, this is the first report of high throughput analyses of sphingolipids and Cers of human TM using standardized mass spectrometric methods.[30,54] The roles of these lipids in TM remain to be elucidated. Consistent with our hypothesis, we found only small variations in the overall sphingolipid and Cer species due to age, sex, race, and drug regime in the donor TM tissues, whereas most of them were common in the control and POAG groups. While further work is necessary to assess the biological consequence of the many lipid species, in this work we have begun laying down a foundation toward the identification and understanding of TM cell and tissue and their aberration in pathologic states.

Acknowledgments

The authors thank Tom Mundorf and Edward Rockwood for TM tissues, Farid Rifai and Maria Carmen Piqueras for their assistance with experiments, and Katyayini Aribindi for her assistance with the manuscript.

Supported in part by National Institutes of Health (Bethesda, MD, USA) Grants EY016112, EY016112S1, and P30-EY14801; the Computational Ocular Genomics Training Grant T32EY023194-01 (GE); a Research to prevent blindness (RPB) career award; and RPB unrestricted grant to University of Miami. The TSQ Quantum Access Max procurement was supported by Department of Defense Grant W81XWH-09-1-0674. The authors alone are responsible for the content and writing of the paper.

Disclosure: **A.J. Aljohani**, None; **G. Edwards**, None; **Y. Guerra**, None; **S. Dubovy**, None; **D. Miller**, None; **R.K. Lee**, None; **S.K. Bhattacharya**, None

References

1. Morrison JC, Acot, TS. In: Morrison JC, Pollack, IP, eds. *Glaucoma Science and Practice*. New York, NY: Thieme Medical Publishers, Inc.; 2003:34–41.
2. Quigley HA, Tielsch JM, Katz J, Sommer A. Rate of progression in open-angle glaucoma estimated from cross-sectional prevalence of visual field damage. *Am J Ophthalmol*. 1996;122:355–363.
3. Quigley HA, Broman AT. The number of people with glaucoma worldwide in 2010 and 2020. *Br J Ophthalmol*. 2006;90:262–267.
4. Gong H, Ruberti J, Overby D, Johnson M, Freddo TF. A new view of the human trabecular meshwork using quick-freeze, deep-etch electron microscopy. *Exp Eye Res*. 2002;75:347–358.
5. Ujiie K, Bill A. The drainage routes for aqueous humor in monkeys as revealed by scanning electron microscopy of corrosion casts. *Scan Electron Microsc*. 1984;849–856.
6. Maepea O, Bill A. The pressures in the episcleral veins, Schlemm's canal and the trabecular meshwork in monkeys: effects of changes in intraocular pressure. *Exp Eye Res*. 1989;49:645–663.

7. Yang CY, Liu Y, Lu Z, Ren R, Gong, H. Effects of Y27632 on aqueous humor outflow facility with changes in hydrodynamic pattern and morphology in human eyes. *Invest Ophthalmol Vis Sci*. 2013;54:5859–5870.
8. Bhattacharya SK, Rockwood EJ, Smith SD, et al. Proteomics reveal Cochlin deposits associated with glaucomatous trabecular meshwork. *J Biol Chem*. 2005;280:6080–6084.
9. Clark R, Nosie A, Walker T, et al. Comparative genomic and proteomic analysis of cytoskeletal changes in dexamethasone-treated trabecular meshwork cells. *Mol Cell Proteomics*. 2013; 12:194–206.
10. Janssen SF, Gorgels TG, Ramdas WD, et al. The vast complexity of primary open angle glaucoma: dsease genes, risks, molecular mechanisms and pathobiology. *Prog Retin Eye Res*. 2013;37:31–67.
11. Kaufman PL. Adenosine 3′,5′-cyclic-monophosphate and outflow facility in monkey eyes with intact and retrodisplaced ciliary muscle. *Exp Eye Res*. 1987;44:415–423.
12. Southren AL, Gordon GG, Munnangi PR, et al. Altered cortisol metabolism in cells cultured from trabecular meshwork specimens obtained from patients with primary open-angle glaucoma. *Invest Ophthalmol Vis Sci*. 1983;24:1413–1417.
13. Anderson PJ, Wang J, Epstein DL. Metabolism of calf trabecular (reticular) meshwork. *Invest Ophthalmol Vis Sci*. 1980;19:13–20.
14. Weinreb RN, Polansky JR, Alvarado JA, Mitchell MD. Arachidonic acid metabolism in human trabecular meshwork cells. *Invest Ophthalmol Vis Sci*. 1988;29:1708–1712.
15. Nishizuka Y. Membrane phospholipid degradation and protein kinase C for cell signalling. *Neurosci Res*. 1992;15:3–5.
16. Nishizuka Y. Intracellular signaling by hydrolysis of phospholipids and activation of protein kinase C. *Science*. 1992;258: 607–614.
17. Serhan CN. Mediator lipidomics. *Prostaglandins Other Lipid Mediat*. 2005;77:4–14.
18. Smith RS, Zabaleta A, Kume T, et al. Haploinsufficiency of the transcription factors FOXC1 and FOXC2 results in aberrant ocular development. *Hum Mol Genet*. 2000;9:1021–1032.
19. Hannun YA, Obeid LM. Principles of bioactive lipid signalling: lessons from sphingolipids. *Nat Rev Mol Cell Biol*. 2008;9: 139–150.
20. Piomelli D, Astarita G, Rapaka R. A neuroscientist's guide to lipidomics. *Nat Rev Neurosci*. 2007;8:743–754.
21. Spijkers LJ, van den Akker RF, Janssen BJ, et al. . Hypertension is associated with marked alterations in sphingolipid biology: a potential role for ceramide. *PLoS One*. 2011;6:e21817.
22. Tamama K, Okajima F. Sphingosine 1-phosphate signaling in atherosclerosis and vascular biology. *Curr Opin Lipidol*. 2002; 13:489–495.
23. Bourbon NA, Sandirasegarane L, Kester M. Ceramide-induced inhibition of Akt is mediated through protein kinase Czeta: implications for growth arrest. *J Biol Chem*. 2002;277:3286–3292.
24. Cuvillier O, Pirianov G, Kleuser B, et al. Suppression of ceramide-mediated programmed cell death by sphingosine-1-phosphate. *Nature*. 1996;381:800–803.
25. Bhattacharya SK. Recent advances in shotgun lipidomics and their implication for vision research and ophthalmology. *Curr Eye Res*. 2013;38:417–427.
26. Aribindi K, Guerra Y, Lee RK, Bhattacharya SK. Comparative phospholipid profiles of control and glaucomatous human trabecular meshwork. *Invest Ophthalmol Vis Sci*. 2013;54: 3037–3044.
27. Aribindi K, Guerra Y, Piqueras MC, et al. Cholesterol and glycosphingolipids of human trabecular meshwork and aqueous humor: comparative profiles from control and glaucomatous donors. *Curr Eye Res*. In press, 2013;38:1017–1026.
28. Schwudke D, Schuhmann K, Herzog R, Bornstein SR, Shevchenko A. Shotgun lipidomics on high resolution mass spectrometers. *Cold Spring Harb Perspect Biol*. 2011;3: a004614.
29. Shevchenko A, Simons K. Lipidomics: coming to grips with lipid diversity. *Nat Rev Mol Cell Biol*. 2010;11:593–598.
30. Yang K, Cheng H, Gross RW, Han X. Automated lipid identification and quantification by multidimensional mass spectrometry-based shotgun lipidomics. *Anal Chem*. 2009;81: 4356–4368.
31. Yang K, Zhao Z, Gross RW, Han X. Identification and quantitation of unsaturated fatty acid isomers by electrospray ionization tandem mass spectrometry: a shotgun lipidomics approach. *Anal Chem*. 2011;83:4243–4250.
32. Bligh EG, Dyer WJ. A rapid method of total lipid extraction and purification. *Can J Biochem Physiol*. 1959;37:911–917.
33. Bradford MM. A rapid and sensitive method for the quantitation of microgram quantities of protein using the principle of protein-dye binding. *Anal Biochem*. 1976;72:248–254.
34. Crane AM, Hua HU, Coggin AD, et al. Mass spectrometric analyses of phosphatidylcholines in alkali-exposed corneal tissue. *Invest Ophthalmol Vis Sci*. 2012;53:7122–7130.
35. Han X, Yang K, Gross RW. Multi-dimensional mass spectrometry-based shotgun lipidomics and novel strategies for lipidomic analyses. *Mass Spectrom Rev*. 2011;31:134–178.
36. Han X. Multi-dimensional mass spectrometry-based shotgun lipidomics and the altered lipids at the mild cognitive impairment stage of Alzheimer's disease. *Biochim Biophys Acta*. 2010;1801:774–783.
37. Amelinckx A, Castello M, Arrieta-Quintero E, et al. Laser trabeculoplasty induces changes in the trabecular meshwork glycoproteome: a pilot study. *J Proteome Res*. 2009;8:3727–3736.
38. Paepens C, De Saeger S, Van Poucke C, et al. Development of a liquid chromatography/tandem mass spectrometry method for the quantification of fumonisin B1, B2 and B3 in cornflakes. *Rapid Commun Mass Spectrom*. 2005;19:2021–2029.
39. Zachariasova M, Lacina O, Malachova A, et al. Novel approaches in analysis of Fusarium mycotoxins in cereals employing ultra performance liquid chromatography coupled with high resolution mass spectrometry. *Anal Chim Acta*. 2010;662:51–61.
40. Pluskal T, Castillo S, Villar-Briones A, Oresic M. MZmine 2: modular framework for processing, visualizing, and analyzing mass spectrometry-based molecular profile data. *BMC Bioinformatics*. 2010;11:395.
41. Benjamin A, Kashem M, Cohen C, et al. Proteomics of the nucleus ovoidalis and field L brain regions of zebra finch. *J Proteome Res*. 2008;7:2121–2132.
42. Sutter E, Roulet FC. Staining Mycobacterium leprae in paraffin sections by the Gomori methenamine-silver method. *Stain Technol*. 1965;40:49–51.
43. Kwon YH, Fingert JH, Kuehn MH, Alward WL. Primary open-angle glaucoma. *N Engl J Med*. 2009;360:1113–1124.
44. Valsecchi M, Mauri L, Casellato R, et al. Ceramide and sphingomyelin species of fibroblasts and neurons in culture. *J Lipid Res*. 2007;48:417–424.
45. Vukelic Z, Kalanj-Bognar S, Froesch M, et al. Human gliosarcoma-associated ganglioside composition is complex and distinctive as evidenced by high-performance mass spectrometric determination and structural characterization. *Glycobiology*. 2007;17:504–515.
46. Zegans ME, Becker HI, Budzik J, O'Toole G. The role of bacterial biofilms in ocular infections. *DNA Cell Biol*. 2002;21: 415–420.

Investigative Ophthalmology & Visual Science

47. Safneck JR. Endophthalmitis: A review of recent trends. *Saudi J Ophthalmol*. 2012;26:181–189.
48. Sforza S, Dall'asta C, Marchelli R. Recent advances in mycotoxin determination in food and feed by hyphenated chromatographic techniques/mass spectrometry. *Mass Spectrom Rev*. 2006;25:54–76.
49. Gelderblom WC, Smuts CM, Abel S, et al. Effect of fumonisin B1 on the levels and fatty acid composition of selected lipids in rat liver in vivo. *Food Chem Toxicol*. 1997;35:647–656.
50. Ibanez C, Simo C, Barupal DK, et al. . A new metabolomic workflow for early detection of Alzheimer's disease. *J Chromatogr A*. 2013;1302:65–71.
51. Gupta S, Maurya MR, Merrill AH Jr, Glass CK, Subramaniam S. Integration of lipidomics and transcriptomics data towards a systems biology model of sphingolipid metabolism. *BMC Syst Biol*. 2011;.5:26.
52. Guerra Y, Aljohani AJ, Edwards G, Bhattacharya SKA. Comparison of trabecular meshwork sphingolipids and ceramides of ocular normotensive and hypertensive states of DBA/2J mice. *J Ocul Pharmacol Ther*. 2014;30:283–290.
53. Mettu PS, Deng PF, Misra UK, et al. Role of lysophospholipid growth factors in the modulation of aqueous humor outflow facility. *Invest Ophthalmol Vis Sci*. 2004;45:2263–2271.
54. Herzog R, Schuhmann K, Schwudke D, et al. LipidXplorer: a software for consensual cross-platform lipidomics. *PLoS One*. 2012;7:e29851.

Investigative Ophthalmology & Visual Science